Pharmaceutical Research, Vol. 25, No. 1, January 2008 (© 2007)
DOI: 10.1007/s11095-007-9400-7

Research Paper

Immunocolloidal Targeting of the Endocytotic Siglec-7 Receptor Using Peripheral Attachment of Siglec-7 Antibodies to Poly(Lactide-*co*-Glycolide) Nanoparticles

Christopher J. Scott,[1] Waleed M. Marouf,[1] Derek J. Quinn,[1] Richard J. Buick,[2] Selinda J. Orr,[3] Ryan F. Donnelly,[1] and Paul A. McCarron[1,4]

Received February 16, 2007; accepted June 28, 2007; published online August 3, 2007

Purpose. To prepare a nanoparticulate formulation expressing variable peripheral carboxyl density using non-endcapped and endcapped poly(lactide-*co*-glycolide), conjugated to antibodies recognising the siglec-7 receptor, which is expressed on most acute myeloid leukaemias. The aim is to exploit this receptor as a therapeutic target by constructing an internalising drug-loaded nanoparticle able to translocate into cytoplasm by siglec receptor-mediated internalisation.
Materials and Methods. Antibodies to the siglec-7 (CD33-like) receptor were conjugated to dye-loaded nanoparticles using carbodiimide chemistry, giving 32.6 μg protein per mg of nanoparticles using 100% of the non-endcapped PLGA. Binding studies using cognate antigen were used to verify preservation of antibody function following conjugation.
Results. Mouse embryonic fibroblasts expressing recombinant siglec-7 receptor and exposed to Nile-Red-loaded nanoparticles conjugated to antibody accumulated intracellular fluorescence, which was not observed if either antibody or siglec-7 receptor was absent. Confocal microscopy revealed internalised perinuclear cytoplasmic staining, with an Acridine Orange-based analysis showing red staining in localised foci, indicating localisation within acidic endocytic compartments.
Conclusions. Results show antibody-NP constructs are internalised via siglec-7 receptor-mediated internalisation. If loaded with a therapeutic agent, antibody-NP constructs can cross into cytoplasmic space and delivery drugs intracellularly to cells expressing CD33-like receptors, such as natural killer cells and monocytes.

KEY WORDS: internalising; intracellular delivery; nanoparticle; natural killer cells; siglec.

INTRODUCTION

The premise behind targeting of nanoparticulate delivery systems is principally one of increasing drug activity and reducing dose by maximising drug availability at the intended cellular site of action. This leads to a hypothetical reduction of unwanted noxious effects brought about by minimising drug exposure to distant healthy sites (1,2). The simplest type of colloidal targeting relies on passive mechanisms, which depend on the biodistribution patterns achieved by the carrier following administration. For example, nanoparticles (NP) with a degree of stealth can accumulate preferentially into the desired site of action by exploiting histological changes evident in disease states that exhibit the enhanced permeation and retention (EPR) effect. This is brought about by a leaky vasculature displayed in tumour types with disrupted endothelial structures (3). Their non-stealth counterparts are rapidly sequestered by the reticulo-endothelial system (RES) located mainly in liver and spleen. Although a possible drawback for most intravenous NP use, such sequestering can be used to target anti-leishmanial-containing NP hepatically and, hence, increase their therapeutic activity by solely passive means (4). Active targeting, on the other hand, differs fundamentally from passive mechanisms in that there is specific affinity displayed at the nanoparticle surface. This affinity derives from an attached moiety, such as a monoclonal antibody, that both recognises and interacts with a particular cell, tissue or organ in the body.

Active targeting of NP to particular sites in the body can be achieved using peripheral ligands that bind specifically to exposed cellular biomolecules expressed with some degree of uniqueness. Upon successful docking, it is reasonable to assume that the NP remains either on the periphery of the cell or is endocytosed. Naked NP and many large molecular weight potent therapeutic agents do not cross the lipid bilayer by passive diffusion alone, a process precluded by

[1] School of Pharmacy, Queens University Belfast, Medical Biology Centre, 97 Lisburn Road, Belfast, BT9 7BL, UK.
[2] Fusion Antibodies Ltd., Springbank Industrial Estate, Pembroke Loop Road, Belfast, BT17 0QL, UK.
[3] Centre for Cancer Research and Cell Biology, Queens University Belfast, Medical Biology Centre, 97 Lisburn Road, Belfast, BT9 7BL, UK.
[4] To whom correspondence should be addressed. (e-mail: p.mccarron@qub.ac.uk)

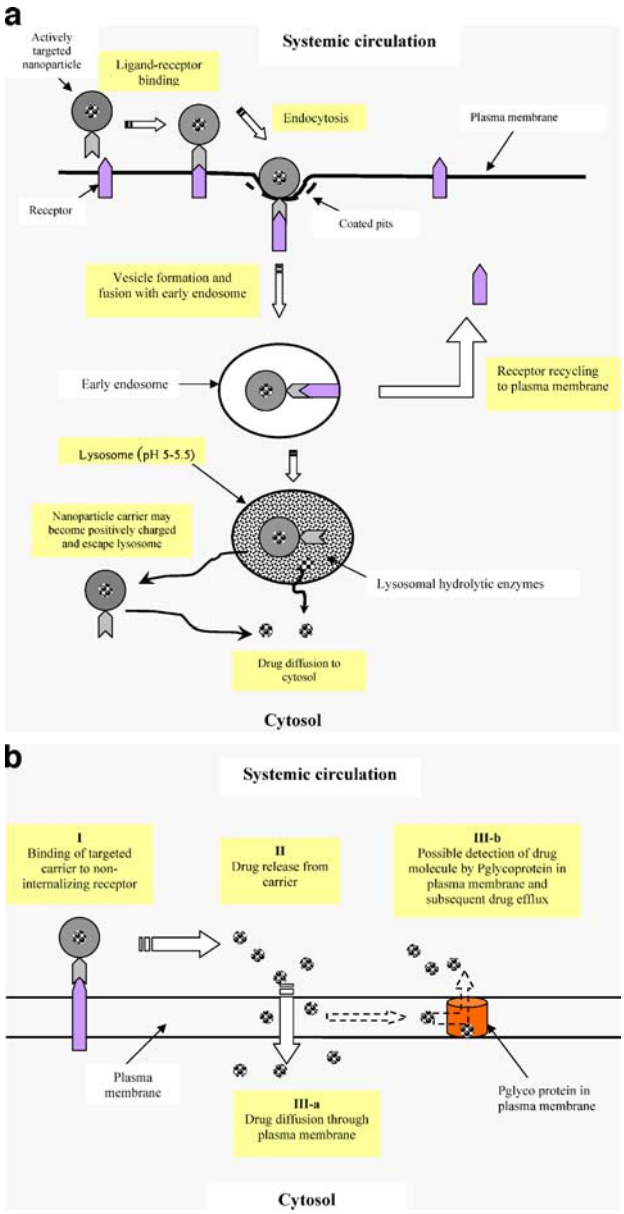

Fig. 1. **a** Schematic presentation showing binding of targeted ligand to an internalising receptor. The colloidal carrier is taken up into lysosome, where it can release its payload or escape into the cytosol. **b** Schematic presentation showing binding of a targeted carrier to non-internalizing receptor where drug released from carrier (I) diffuses to the cytosol through the plasma membrane, (II) is detected by *P*-glycoprotein in the plasma membrane which is responsible for (III) drug efflux and resistance.

their inherent size. To achieve intracellular delivery of difficult drugs, a strong case can be made for constructing a generic NP able to carry predefined payloads and able to interact with an internalising surface receptor. This receptor-mediated internalisation is illustrated in Fig. 1a and permits colloidal material direct assess to the cytoplasm. For therapies, such as those using immunoliposomes, endocytosis is necessary for optimal results (5). For other therapies, such as antibody-directed enzyme-prodrug therapy (ADEPT), it is important that endocytosis does not occur because the enzyme must be present at the cell surface to convert non-active prodrugs into active cytotoxic molecules (6).

Previously, it has been demonstrated that PLGA NP targeted against internalising receptors have increased therapeutic activities in specific tumour models. Lim and Mo (7) demonstrated that wheat germ agglutinin-receptor mediated endocytosis potentiated the anticancer activity of placlitaxel against malignant pulmonary cell lines. In a similar strategy, targeting of prostate-specific membrane antigen with a NP-aptamer bioconjugate resulted in internalisation and intracellular delivery of docetaxel and enhanced activity against prostate cancer cell lines (8). Park *et al.* (9) demonstrated a high increase in therapeutic index of doxorubicin encapsulated in anti-HER2 immunoliposomes, both by reducing side effects and increasing the anti-tumour activity in HER2 overexpressing tumour xenograft animal models. This work also suggested that NP possessed an advantageous ability of overcoming efflux generated by P-glycoprotein pumping (Fig. 1b), which acts upon drug in the plasma membrane. Since drug entrapped within NP are essentially hidden from such mechanisms, an internalised carrier is able to bypass this mechanism and be in a position to release drug within the cytosol (10).

One suitable family of membrane targets that display internalisation upon ligand binding are the siglec family of inhibitory receptors (11). They are a distinctive subset of the Ig superfamily and possess a structure considered to be adhesion-molecule like. They are cell surface receptors, recognising sialic acids and expressed predominantly in cells belonging to the haemopoietic and immune systems (12). Siglecs (or "siglec receptors" as both terms are synonymous) comprise sialoadhesin (siglec-1/Sn), CD22 (siglec-22), CD33 (siglec-3) and myelin-associated glycoprotein (MAG or siglec-4). The siglec receptors ranging from siglec-5 to siglecs-11 are known as CD33-related siglecs (13,14). Upon activation, these receptors are internalised (11) and degraded through the proteasome in a SOCS-3 dependent manner (15).

Siglec-7 receptor is expressed on human natural killer (NK) cells and monocytes. The cytotoxicity of NK cells is inhibited by clustering siglec-7 receptor with sialic ligands on the cell surface (16) or with cross-linking antibodies (17). Moreover, it has also been shown that antibody-induced cross-linking of CD33-related siglec receptors, such as siglec-7 receptor, can result in apoptosis and reduced proliferation in leukaemia cells (18–20). The exploitation and targeting of siglec receptors has formed the basis of the commercialised antibody-based product Mylotarg® (gemtuzumab ozogamicin; Wyeth Laboratories, Philadelphia, PA) for the treatment of acute myeloid leukaemia (AML). Gemtuzumab ozogamicin consists of calicheamicin, a potent antibiotic, conjugated to a humanised anti-CD33 monoclonal antibody. CD33 is expressed on the surface of leukaemic blast cells in more than 80% of patients with AML (21) and so it is readily amenable as a therapeutic target for site-specific capable drug delivery systems. Engagement of CD33 by gentuzumab ozogamicin results in internalisation of the immunoconjugate, culminating in the release of the DNA damaging agent calicheamicin (22). AML cells express varying degrees of multiple CD33-related siglecs and while CD33 is expressed on a high percentage of AML cells, it is not expressed on all. Similarly, siglec-7 receptor is relatively highly expressed on

Table I. Nanoparticulate Diameter, Polydispersity, Zeta Potential and Anti-Siglec-7 Conjugation

Proportion of RG 502 H in the NP PLGA Core (%)	Average Size (nm)±SD[a]	Polydispersity[a]	Zeta Potential (mV)	Anti-Siglec-7 Conjugation[b] (μg mg^{-1})
Blank nanoparticles				
20	119.6±1.0	0.070±0.007	3.1±0.0	17.1±2.6
100	110.1±1.6	0.072±0.003	3.1±0.0	32.6±2.3
Nile Red-loaded				
20	122±1.2	0.080±0.007	3.1±0.0	17.6±2.1
100	112±1.1	0.054±0.006	3.3±0.0	33.3±1.5
Acridine Orange-loaded				
20	120.4±0.8	0.080±0.005	3.3±0.0	17.3±1.9
100	111.2±1.5	0.090±0.009	3.2±0.0	31.9±2.8

[a] Mean and standard deviation of three determinations
[b] Antibody conjugation is expressed as average of three determinations in micrograms per gram of antibody per milligram of activated nanoparticle±standard deviation.

some subtypes of AML and may, therefore, be considered as a possible target in combination with CD33 or other siglec receptors for antibody based therapies (23).

The approach taken in this work was to target the siglec-7 receptor, a member of a family of receptors previously shown to internalise upon attachment. An aim was to construct a biodegradable poly(lactide-*co*-glycolide) (PLGA) NP with an attached peripheral antibody recognising the siglec-7 receptor. A second aim was to investigate if binding of this antibody-NP complex to the siglec receptor could be achieved and whether this would result in internalisation, thus delivering the entrapped payload directly into the cell. Specifically, the PLGA NP will be loaded with a fluorescent dye (Nile Red) so that a study of the cellular nanoparticulate uptake can be made. Furthermore, NP, loaded with Acridine Orange, a pH sensitive fluorescent dye, will be used to investigate further if NP are internalised into acidic endosomal compartments.

MATERIALS AND METHODS

Materials

PLGA (Resomer® RG 502 H; acid value 9 mg KOH per g; molecular weight 12 KD) was a generous gift from Boehringer Ingelheim, Germany. PLGA (Resomer® RG 505 S, acid value <1 mg KOH per g PLGA, molecular weight 80 KD) was purchased from Boehringer Ingelheim, Germany. *N*-(3-Dimethylaminopropyl)-*N*-ethyl carbodiimide hydrochloride (EDC) was obtained from Fluka, Slovakia. *N*-Hydroxy succinimide (NHS) and poly(vinyl alcohol) (PVA) 87–89% hydrolyzed with average molecular weight 13,000–23,000 was obtained from Aldrich Ltd., Germany. Magnesium chloride hexahydrate (ACS reagent), 2-morpholinoethanesulfonic acid (MES) buffer and Nile Red (NR) were purchased from Sigma Ltd., Germany. Anti-siglec-7 polyclonal antibody (150 kDa—affinity purified immunoglobulin) and siglec-7 recombinant antigen (N-terminal extracellular domain, residues 20–125) were supplied by Fusion Antibodies Ltd., Northern Ireland. Acridine Orange (AO) was obtained from Sigma Ltd., USA. Phenol Red free medium (RPMI 1640 with L-Glutamine) and McCoy's 5A medium with L-Glutamine were obtained from Invitrogen/Gibco Ltd., USA. Mouse Embryonic Fibroblast (MEF) cell lines were obtained from the American Tissue Culture Collection. Solvents used in this work were of HPLC grade and used without further purification. All other materials were of appropriate laboratory grade.

Preparation and Characterisation of Fluorescently Labelled PLGA NP Cores

PLGA RG 502 H, either alone (100% w/w) or as a 20% w/w physical mixture with RG 505 S, was dissolved (total weight 100 mg) in 4.0 ml of organic phase, comprising a 3:1 v/v acetone/dichloromethane (DCM) mix. Nile Red was added to the organic phase at a ratio of 1:100 w/w to PLGA and injected under moderate stirring into 15 ml of an ice-cold aqueous phase (pH 5.0; 25 mM MES buffer) containing 2.5% w/v PVA and 45% w/v $MgCl_2.6H_2O$. Both phases were then sonicated in an ice bath for 3 min, at 50–55 W in pulse mode. An additional 20.0 ml of 2.5% w/v PVA solution made up in 25 mM MES buffer (pH 5.0) was added under moderate stirring to initiate acetone diffusion. Samples were kept stirring overnight to allow evaporation of the organic component.

The preparation of Acridine Orange-loaded NP followed the method used for those loaded with Nile Red, but with some modifications. Acridine Orange (1.0 mg) was dissolved in 500 μl DMSO and added to 3.5 ml of ice-cold organic phase, consisting of PLGA (100.0 mg) dissolved in 2.5 ml acetone and 1.0 ml DCM. The remaining part of the method was identical to that described above. Blank NP containing no dye payload were prepared in a similar way to that used to manufacture Nile Red-loaded NP, but without inclusion of the dye substance to the organic phase.

NP were filtered through a No. 1 sintered glass filter, centrifuged at 50,000×*g* for 1 h at 10°C, then washed three times using suspension-spin cycles with pH 5.0 MES buffer. This was to eliminate any loosely adsorbent materials or free dye. In the case of Acridine Orange, NP were washed until a clear supernatant was evident. Nanoparticulate pellets were resuspended at 1.0 mg ml^{-1} in pH 5.0 MES buffer prior to further use.

Nanoparticulate size, zeta potential and polydispersity were measured using photon correlation spectroscopy (Zeta-

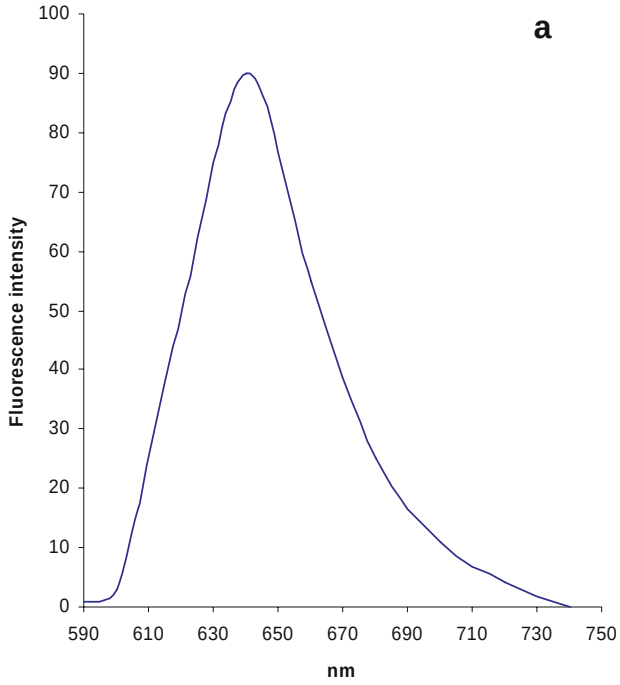
a
Fluorescence intensity
nm

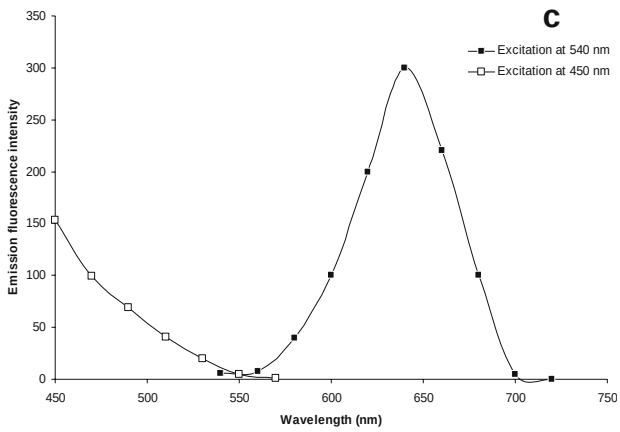
c
Excitation at 540 nm
Excitation at 450 nm
Emission fluorescence intensity
Wavelength (nm)

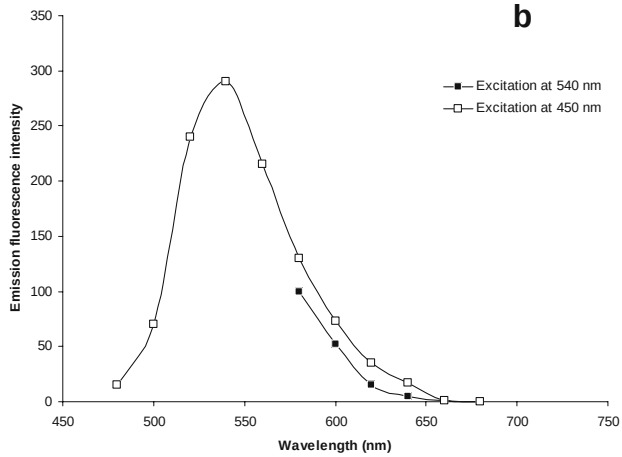
b
Excitation at 540 nm
Excitation at 450 nm
Emission fluorescence intensity
Wavelength (nm)

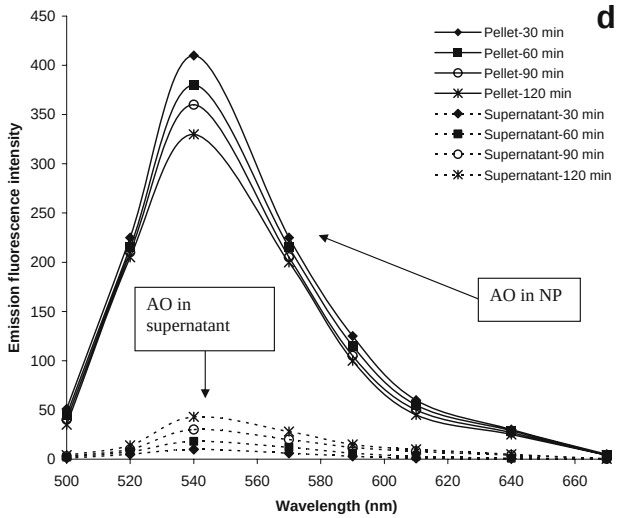
d
Pellet-30 min
Pellet-60 min
Pellet-90 min
Pellet-120 min
Supernatant-30 min
Supernatant-60 min
Supernatant-90 min
Supernatant-120 min
AO in supernatant
AO in NP
Emission fluorescence intensity
Wavelength (nm)

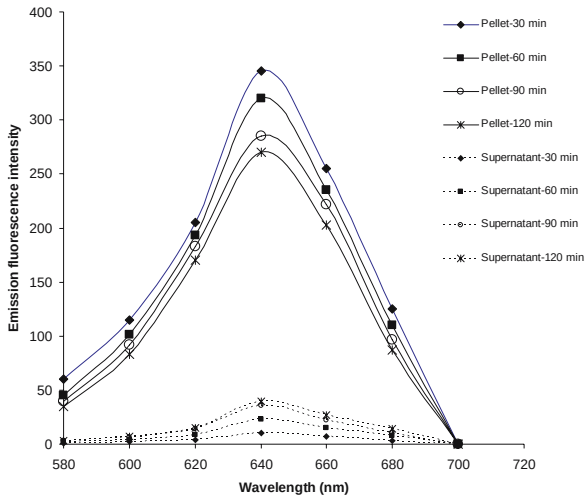
e
Pellet-30 min
Pellet-60 min
Pellet-90 min
Pellet-120 min
Supernatant-30 min
Supernatant-60 min
Supernatant-90 min
Supernatant-120 min
Emission fluorescence intensity
Wavelength (nm)

◀ **Fig. 2.** Fluorescence emission spectra of **a** Nile Red-loaded NP (excitation 540 nm), **b** Acridine Orange-loaded NP suspended in pH 7.4 PBS, showing green fluorescence (excitation 450 nm) and little red fluorescence when excited at either 450 or 540 nm and **c** Acridine Orange-loaded NP suspended in pH 5.0 MES buffer showing red fluorescence (excitation 540 nm). Time-related changes in emission spectra obtained during release experiments are shown for AO detected in both supernatant and pellet fractions at **d** pH 7.4 (excitation 450 nm) and at **e** pH 5.0 (excitation 540 nm).

Sizer 3000 HS, Malvern instruments, UK). Measurements were carried out at room temperature (25°C), with each sizing determination done in triplicate and an average particle size expressed as the mean diameter (Z_{ave}). Fluorescence spectra of NR-loaded NP were recorded by suspending in PBS (pH 7.4) and using excitation at 540 nm. The fluorescence spectra of AO-loaded NP at neutral conditions were recorded by suspension in PBS (pH 7.4) and using two excitation wavelengths at 450 and 540 nm. The fluorescence spectra of AO-loaded NP in acidic conditions were recorded by suspension in MES buffer (pH 5.0) and using excitation at 540 nm. Of particular interest in these analyses was the magnitude of a red signal in the spectra. The fluorescence spectrum of AO-loaded NP in neutral environments was recorded by suspending in PBS (pH 7.4) and using excitation at 540 nm.

The possible premature release of AO from loaded NP over the typical duration of a cell exposure study (90 min) was evaluated using a drug release type experiment. AO-loaded NP were washed extensively to remove surface drug and suspended in PBS (pH 7.4) and MES (pH 5.0) media. At 30, 60, 90 and 120 min, the NP were separated from the continuous phase by centrifugation (100,000×*g*) and the fluorescence in both phases assessed. Release of NR was not investigated as its release into aqueous receiver phases over 4 h is negligible (data not shown).

NP Activation and Peripheral Attachment of Anti-Siglec7 Polyclonal Antibody

Purified NP (containing 100.0 mg PLGA), suspended in 10 ml pH 5.0 MES buffer, were activated using NHS-carbodiimide chemistry. The pH was maintained at 5.0 in order to maximise attachment at carboxylic acid groupings pendent from superficial PLGA. Activation was achieved by adding 1.0 ml of 0.1 M EDC and 1.0 ml of 0.7 M NHS, both dissolved in pH 5.0 MES, to the nanoparticulate suspension (24), which was kept at room temperature for 1 h under conditions of moderate stirring. Samples were centrifuged at 50,000 *g* for 1 h at 10°C, the NP collected, washed three times in phosphate buffered saline to eliminate unused adsorbent reagents and finally resuspended at 1.0 mg ml^{-1} in pH 7.4 phosphate buffered saline.

Anti-siglec-7 polyclonal antibody solution (100 µl of 0.5 mg ml^{-1}) was added to 1.0 ml suspension of 1.0 mg ml^{-1} activated NP in pH 7.4 PBS and then incubated at 4°C for 24 h. Conjugated NP were centrifuged for 60 min at 22,000 g (Sigma 3–18 K Centrifuge) at 5°C to remove excess unconjugated antibody and washed for a further two suspension–spin cycles with pH 7.4 PBS. Controls were prepared in a similar fashion using PLGA NP that had not been subjected to carbodiimide activation.

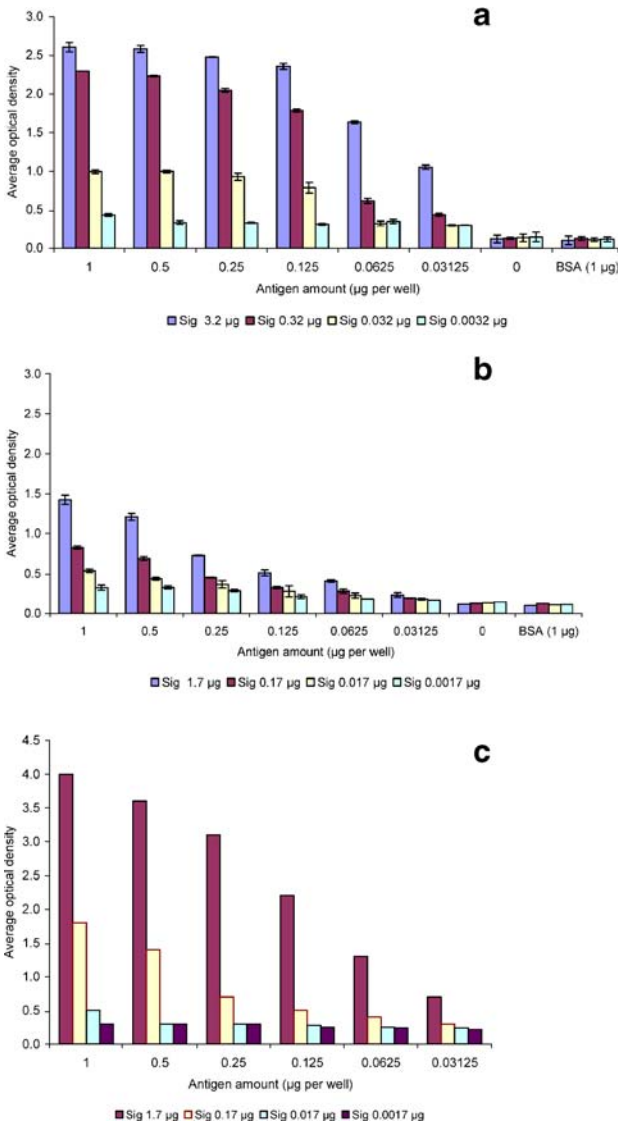

Fig. 3. ELISA for anti-siglec-7 polyclonal antibody activity following conjugation to NP manufactured from **a** 100% RG 502 H PLGA, **b** 20% RG 502 H PLGA and **c** for free anti-Siglec-7 polyclonal antibody. In the legend for subpanels **a** and **b**, Sig 1.7 µg indicates a concentration of 1.7 µg protein per mg NP and so on. In subpanel **c**, this legend refers to free antibody.

The amount of antibody conjugated to NP was evaluated by quantifying protein attached to the surface of the NP using the bicinchoninic acid (BCA) assay (Micro BCA Protein Assay Kit, Pierce Ltd., USA). A working reagent was prepared by mixing 25 parts of micro BCA™ reagent MA (sodium carbonate, sodium bicarbonate and sodium tartarate in 0.2 N NaOH) and 24 parts reagent MB (4% BCA in water) with 1 part of reagent MC (4% cupric sulfate pentahydrate in water). Each standard or unknown sample (150.0 µl) was added to a microplate well containing 150.0 µl of the working reagent. All samples were done in triplicate. The plate was thoroughly mixed on a plate shaker for 30 s, covered, incubated at 37°C for 2 h and analysed spectrophotometrically at 562 nm (Tecan Spectra III, Austria) and compared to standard calibration curves for bovine serum albumin. Blank NP, previously activated with EDC/NHS and washed thrice in phosphate buffered saline, were

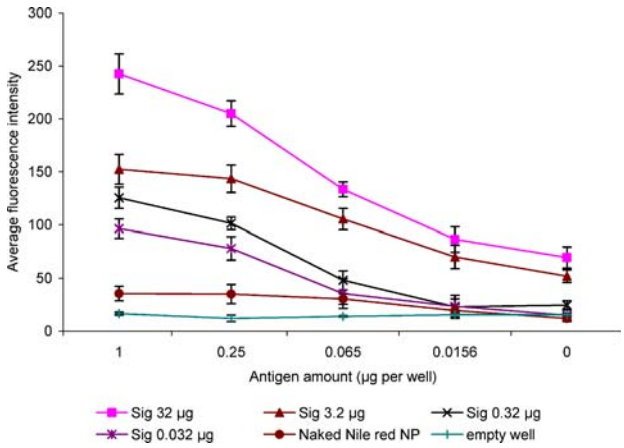

Fig. 4. Fluorescent immunosorbent assay for anti-siglec-7 polyclonal antibody conjugated to NR-loaded PLGA (100% RG 502 H) nanoparticles. In the legend, Sig 32 µg indicates a concentration of 32 µg protein per well and so on.

used as negative controls to ensure no interferences in the assay procedure.

ELISA-based Procedures

Purified siglec-7 antigen was coated onto Maxisorb® 96-well plates (Nunc, Denmark). The wells were coated with antigen (0.0 µg to 1.0 µg) in 100 µl coating buffer (50 mM sodium bicarbonate buffer, equilibrated to pH 9.5 with 50 mM sodium carbonate) for 1 h at 37°C. The coated wells were washed thoroughly with 0.2% w/v Tween 20 dissolved in pH 7.4 PBS and then blocked with 5% dried milk powder in PBS for 1 h at 37°C. Samples (100 µl) equivalent to 3.2000, 0.3200, 0.03200 and 0.0032 µg of anti-siglec-7 polyclonal antibodies conjugated to NP were applied to these wells (dilution series prepared in a 0.2% w/v Tween 20 solution in pH 7.4 PBS) and the plates incubated with shaking at room temperature for 1 h. After further washing as before, the bound siglecs-7 antibody was disclosed using a secondary antibody of goat α-mouse-HRP (Horse Radish Peroxidase) (Sigma, Poole UK) at a dilution of 1:3000, which was also incubated with shaking at room temperature for 1 h. Following a further thorough washing with a 0.2% w/v Tween 20 dissolved in pH 7.4 PBS, bound goat α-mouse-HRP was quantified by the addition of 100 µl of tetramethylbenzidine (TMB) to each well. After 30 min at 37°C, the reaction was stopped by addition of 50 µl 1.0 M HCl and the colorimetric results determined spectrophotometrically (Tecan Spectra III, Austria) at a wavelength of 450 nm. Controls were performed by adding siglec-7-conjugated NP to wells pre-coated with 1.0 µg of bovine serum albumin (BSA) and to empty wells.

ELISA for anti-siglec-7 polyclonal antibodies conjugated to Nile Red-loaded NP began by coating siglecs-7 antigen to black Maxisorb® plates, as described above. The coated wells were washed thoroughly with a 0.2% w/v Tween 20 dissolved in pH 7.4 PBS and then blocked with 5% dried milk powder in PBS for 1 h at 37°C. Samples (100 µl) equivalent to 3.2000, 0.3200, 0.0320 and 0.0032 µg anti-siglec antibody per mg of NP were added to wells containing different amounts of antigen. Controls were performed by adding anti-siglec-7-conjugated NP to wells pre-coated with 1.0 µg of bovine serum albumin (BSA), as well as to empty wells. Plates were agitated gently by shaking (100 rpm) at room temperature for 2 h before disclosing bound siglec-7 antibody using goat α-mouse-HRP at a dilution of 1:3000. Bound goat α-mouse-HRP was quantified using tetramethylbenzidine with results determined spectrophotometrically at 450 nm, as described above. The fluorescence intensity of Nile Red-loaded NP was measured using a multi-well plate reader (Cytoflour Series 4000, PerSeptive Biosystems USA) with excitation and emission wavelengths of 485 nm and 620 nm, respectively.

Cell Culture and Transient Transfection Studies

Mouse embryonic fibroblast cells (MEF), obtained from American Tissue Culture Collection (ATCC), were cultured on Phenol Red-free RPMI medium with L-glutamine and 10% fetal calf serum (FCS) and grown on glass cover slips in 35 mm diameter Petri dishes to a confluency of 70%. Cells were transfected transiently either with siglec-7 (open reading frame) cDNA in pMX-IRES-EGFP plasmid, as described previously (13) (1.0 µg), or with empty vector using Metafectene™ reagent according to manufacturers instructions (Biontex Laboratories GmbH, Germany). Monolayers, after 48 h post-transfection, were subjected to a 90-minute period of incubation (37°C, 5% CO_2) with a 100 µl dispersion of 1.0 mg ml^{-1} Nile Red-loaded or Acridine Orange-loaded NP suspended in PBS. Both dye-loaded variants contained 32.0 µg anti-siglec-7 polyclonal antibodies conjugated to NP surface, with naked dye-loaded NP acting as corresponding controls. Cells were washed three times with ice-cold PBS before observation using confocal scanning laser microscopy (Leica Confocal Sytem TCS Sp2, Germany). A laser wavelength of 540 nm was used for the excitation of the red fluorescence of Nile Red. For Acridine Orange-loaded NP, excitation was set at 450 and 540 nm for green and red fluorescence respectively.

Statistical Analysis

The statistical analysis was performed using analysis of variance (one-way ANOVA) followed by the Bonferroni's test to compare all pairs of preparations, using Graph-Pad Prism (San Diego, CA, USA). Rejection of the null hypothesis was considered with P values<0.05.

RESULTS

Mean sizes and zeta potentials for blank, Nile Red (NR)-loaded and Acridine Orange (AO)-loaded and purified NP are shown in Table I. The PLGA mix used in this study determines the carboxyl density on the NP surface, with low carboxylic acid surface density achieved using 20% RG 502 H w/w in the total PLGA blend, while a maximal surface density was obtained using 100% RG 502 H. The results presented in Table I show that NP with an average size of less than 200 nm were typical of the preparation methods used, regardless the type of PLGA comprising the NP matrix (P>0.05). However, NP prepared from 20% RG 502 H were approximately 10 nm bigger than those prepared from 100%

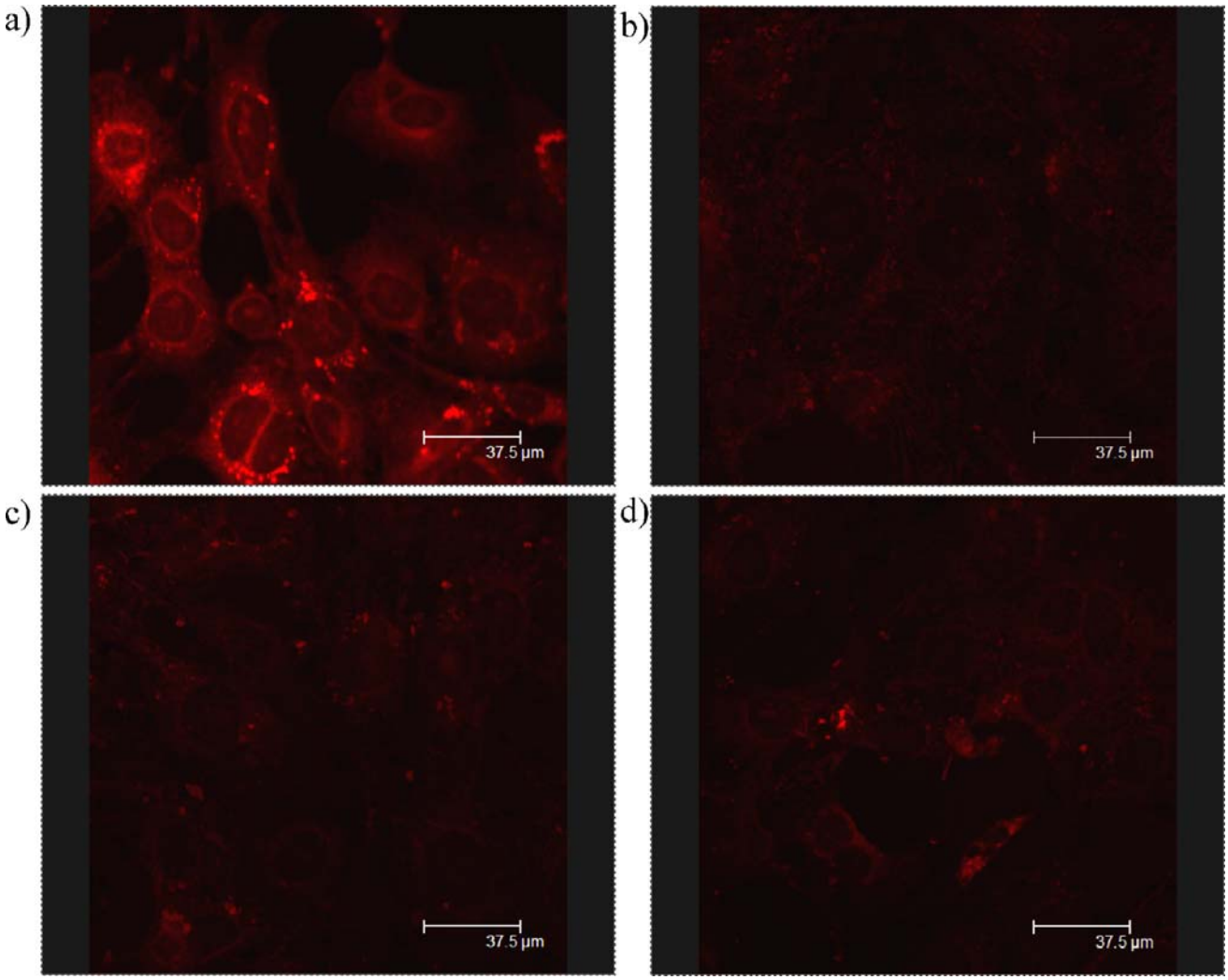

Fig. 5. Fluorescent cell microscopy images (X800) of mouse embryonic fibroblasts (MEF) cells, grown to a confluency of 70% and exposed to NR-loaded NP prepared using 100% PLGA RG 502 H; **a** MEF cells expressing siglec receptor and incubated with Nile Red loaded nanoparticles conjugated to anti-siglec-7 polyclonal antibody; **b** MEF cells without siglec receptor and incubated with Nile Red loaded nanoparticles conjugated to anti-siglec-7 polyclonal antibody; **c** MEF cells expressing siglecs-7 receptor and incubated with naked Nile Red loaded nanoparticles; **d** MEF cells without siglec-receptor and incubated with naked NR-loaded NP.

RG 502 H. Furthermore, results in Table I also demonstrate that inclusion of either NR or AO dye did not affect size or charge characteristics ($P>0.05$). The size distribution was shown to be monomodal, as verified by the low polydispersity value, which in all cases was less than 0.10. Although the yield was not determined in this work, close inspection of the nanoparticulate dispersion following preparation did not uncover debris nor show indications of aggregation. This was strong evidence that yields were good.

The fluorescent emission spectra arising from the encapsulated dye materials were determined by excitation of the respective dilute nanoparticulate suspensions. Thus, the spectrum from NR-loaded NP was evaluated by studying emission from nanoparticulate suspensions using excitation at 540 nm. Fig. 2a shows maximum emission intensity was observed at 640 nm. In a similar fashion, the fluorescence of AO-loaded NP was evaluated, but at two different pH values, done by suspension in pH 7.4 (PBS) and pH 5.0 media (MES buffer). It is known that the emissive properties of AO change in response to environmental pH and the fluorescence emission spectrum at pH 7.4 can be seen in Fig. 2b. Clearly, at neutral pH, AO-loaded NP fluoresce strongly in the green region, peaking around 540 nm, with little red fluorescence exhibited around 640 nm Similarly, when excited at 540 nm, the spectrum verifies that there is little emission beyond 630 nm. This can be contrasted with NP suspended in pH 5.0 media and excited at 540 nm, where intense red emission with a maximum at 640 nm is evident, as shown in Fig. 2c. Also, in this figure, excitation at 450 nm does not produce fluorescent emission at 630 nm.

Fig. 2d, e shows that the majority of the fluorescence remains in the NP over a period of 120 min. There is some reduction in the NP fluorescence as AO leaks into the continuous phase, but the majority of fluorescence signal is coming from dye-loaded NP. This release pattern is seen for NP suspended in both media (pH 5.0 and 7.4). The spectra of free AO in solution and of AO entrapped in NP are of identical shape, again an effect seen in both release media. Thus, the fluorescent spectra seen in Fig. 2b, c are originating predominantly from AO that is still entrapped in the NP.

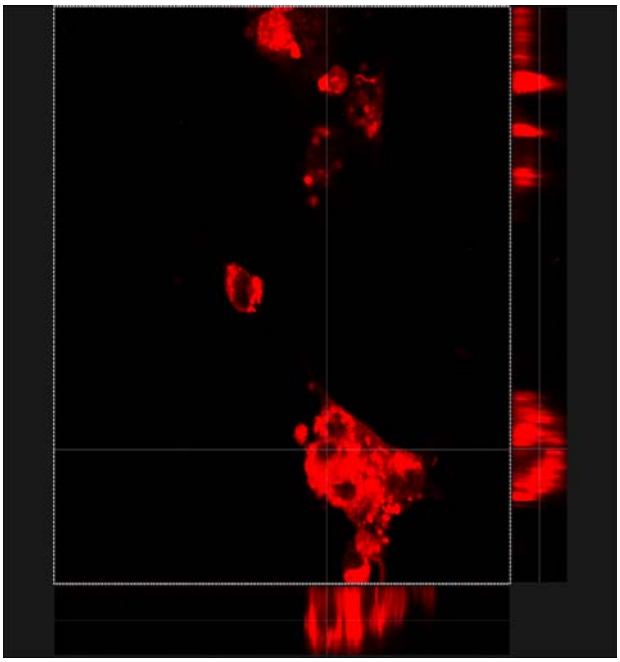

Fig. 6. Confocal fluorescent cell microscopy images for X/Y Y/Z section analysis of MEF cells expressing siglec receptor and incubated with 100 μl PBS dispersion of 1.0 mg ml^{-1} Nile Red loaded nanoparticles conjugated with 32 μg anti-siglec-7 polyclonal antibody at 37°C, 5% CO_2 for 90 min. Cells were washed three times with ice cold PBS before observation using a confocal scanning laser microscopy. Intense red fluorescence observed around nucleolus (black area within cells) is indicative of cytoplasmic presence of Nile Red loaded nanoparticles rather than adsorption to cell surface.

Further consideration of the results in Fig. 2b, c preclude the possibility of a NP core that fluoresces differently to its periphery. NP suspended in pH 5.0 medium emit red fluorescence and do not possess a green emitting core that should be excited using light of 450 nm. Therefore, this NP is unlikely to exist as a green emitting core surrounded by an acidic red shell.

The evaluation of the peripheral attachment of the siglec-7 antibodies was performed by quantifying levels of total protein conjugation and evaluation of its bioactivity by monitoring the ability of conjugated antibody to bind to its cognate antigen. Antibody was conjugated to purified NP using a two-step process of carbodiimide activation followed by antibody attachment. The conjugation efficiency for anti-siglec-7 was found to be dependent on the PLGA composition used to prepare the NP core, as shown in Table I. When NP were prepared using 100% w/w RG 502 H, up to 32.6 μg per mg NP was possible. Reducing the surface density of superficial carboxylic acids, achieved by reducing the percentage of RG 502 H to 20% w/w, resulted in a reduction of anti-siglec7 conjugation to 17.1 μg/mg NP. It was observed that antibody conjugation was not affected by fluorescent dye loading and remained constant for blank nanoparticles and nanoparticles prepared with dyes ($P>0.05$).

The results in Fig. 3 detail the binding of conjugated antibody to immobilised antigen using absorbent microplates. NP were prepared with either 100 or 20% RG 502 H in an attempt to alter surface carboxyl density and vary antibody presentation, a approach already shown to be valid (Table I). A normal sigmoidal relationship between antibody concentration and antigen binding was observed, indicative of antibody-antigen binding. The selectivity of the siglec-7 antibody to its cognate antigen was demonstrated by the low optical densities (around 0.1) measured when bovine serum albumin was replaced as antigen. Even at the high amounts used (1.0 μg per well), the optical density remained almost undetectable and this was still the case as the amount of antibody used was increased. Empty wells treated with antibody conjugated NP also displayed low optical densities, indicating low background adsorption to the Maxisorp layer in the wells.

A more detailed examination of Fig. 3a shows that the optical density profile obtained using 0.0032 μg anti-siglec-7 did not vary as the antigen amount was changed, staying at approximately 0.5. This lack of response in optical density is observed with all concentrations of anti-siglec used provided the amount of antigen remained below about 0.007 μg per well. Beyond this antigen loading, then clear divergent patterns are observed as a stronger response is seen in optical density. For example, using 3.2 μg anti-siglec-7 shows the strongest response, up to an optical density of approximately 2.6. In Fig. 3b, where anti-siglec-7 was conjugated to a lower surface concentration, similar binding profiles were observed. Interestingly though, divergence is seen almost immediately as antigen is presented in the wells. At antigen levels of 0.5 μg, there was a strong positive correlation with measured optical density, indicating both effective and specific binding. At much lower levels of antigen, for example around 0.03 μg per well, the response is unsurprisingly less. The final part of the Fig. 3c shows the activity of the free antibody. The free antibody is seen to be more active and that conjugation to the NP surface has attenuated activity. As an approximation, a comparison between Fig. 3b and 3c would place this attenuation at 90%, leaving approximately 10% of the free activity.

As it is possible that the variations in optical density obtained in ELISA-based procedures could arise from antibody desorbed from the NP and not the intact immunonanoparticle, a further determination using NR-loaded NP was performed. As NR is water-insoluble dye, its premature release from PLGA does not occur and so any antigen interactions with antibody attached to a NR-loaded NP are clearly indicated by total fluorescence in individual wells. The fluorescence intensities captured in Fig. 4 show antibody-antigen concentration dependent in a similar manner to those in Fig. 3. There is a strong relationship between fluorescence and anti-siglec-7 antigen combinations, especially when both are elevated. The low fluorescence intensities obtained in empty wells (0 μg antigen) again verify the low affinity of NP to the Maxisorp layer coating the base of the test wells.

An evaluation was made of recognition and binding capabilities of the immunonanoparticle directed towards the siglec-7 receptor, over-expressed on the cell surface of mouse embryonic fibroblasts (MEF). The fluorescent images in Fig. 5 suggests that MEF cells expressing recombinant siglec-7 receptor and exposed to NR-loaded NP conjugated to antibody are able to localise to the cell surface of the cells. In the absence of antibody conjugation and siglec-7 receptors

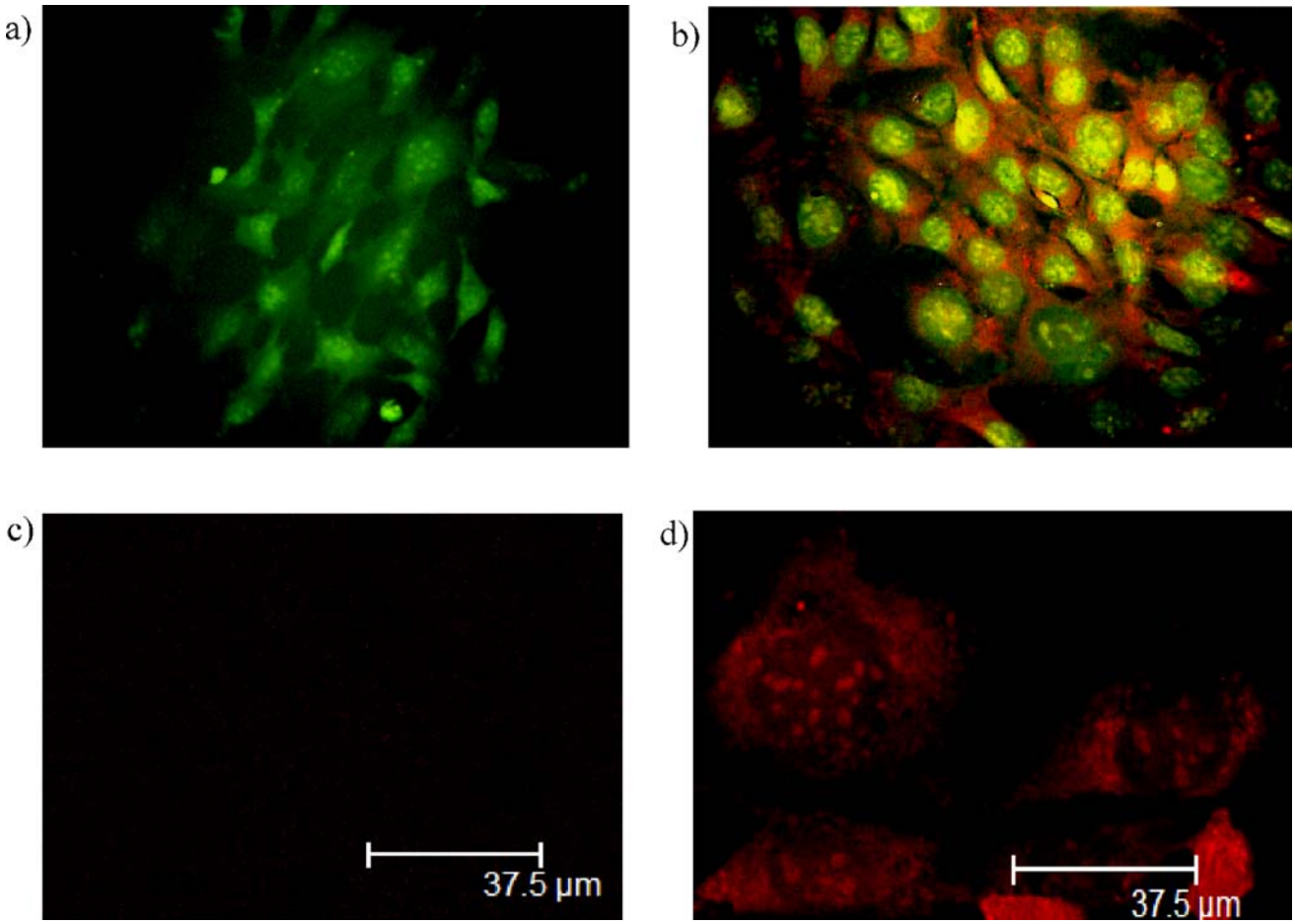

Fig. 7. Fluorescent cell microscopy images for MEF cells expressing siglec receptor and incubated with 100 μl PBS dispersion of 1.0 mg ml−1 of Acridine Orange loaded nanoparticles prepared using 100% PLGA RG 502 H and conjugated with 32 μg anti-siglec-7 polyclonal antibody; **a** MEF cells (X400) without siglec receptor and incubated with anti-siglec-7 conjugated to AO-loaded NP visualised for both red and green emission; **b** MEF cells (X400) expressing siglec receptor and incubated with anti-siglec-7 antibody conjugated to AO-loaded NP visualised for both red and green emission; **c** red fluorescence only for MEF cells without siglec receptor and incubated with anti-siglec 7 conjugated to Acridine Orange loaded nanoparticles; **d** red fluorescence only MEF cells expressing siglec receptor and incubated with anti-siglec 7 conjugated to Acridine Orange loaded nanoparticles Green fluorescence observed in subpanels **a** and **b** is due to presence of green fluorescent protein used in the selection of positive retrovirally infected MEF cells.

in the experimental conditions, little cell associated fluorescence was observed, although some fluorescent artefactual hotspots are discernible. This may arise from non-specific binding arising from hydrophilic interactions with the cell membrane. Some fluorescence was detected in control cells (panels b and c), but again it was noticeably less than that in Fig. 5a. Furthermore, an X/Y Y/Z confocal section analysis, which allows the generation of a 3D graphical representation of the cells was performed. As shown in Fig. 6, the NR fluorescent staining confirms not only localisation of the particles at the cell surface but also internalised perinuclear cytoplasmic staining (Fig. 6). Although the qualitative data in Fig. 5 shows that internalisation is occurring, gathering more substantive data based on quantitative measures of Nile Red fluorescence would represent a logical progression in the work.

Finally, NR was replaced with another fluorescent dye, Acridine Orange (AO). This marker is frequently employed to study subcellular acidic compartments by fluorescent microscopy, as its emission spectra alters from green to red upon acidification. When MEF cells expressing siglec-7 were treated with AO-loaded unconjugated NP and visualised for green and red fluorescence emission there was no detectable red AO fluorescence (Fig. 7a). However, in the presence of conjugated siglec-7 antibody NP marked fluorescence at this wavelength was observed, as shown in Fig. 7b.

While the unconjugated naked NP resulted in no detectable levels of red fluorescence within the cells, when antibody was conjugated to the NP, red AO staining in localised foci within the cytosol was visualised indicative of acidified lysosomal staining. The green fluorescence observed for both conditions is likely a result of the green fluorescent protein (GFP) used in the selection of positive retrovirally infected MEF cells.

DISCUSSION

There are distinct therapeutic advantages to be gained by targeting a drug-loaded NP to a target cell population.

Where the molecular target of the drug is an intracellular target, the therapeutic efficiency of such delivery systems will be improved by the translocation of the NP through the cell membrane and into the cytosol of these cells, before substantive drug release occurs. Thus, the approach described in this work offers a means to gain entry into the target cell that is primarily dependent on the surface chemistry of the NP. The physiochemical properties of the drug are no longer relevant in this respect and become independent of the drug delivery process, that is, until nanoparticulate erosion begins. Therefore, this approach based on one NP formulation could be used conceivably to deliver a wide range of payloads. Furthermore, due to the high concentration of the drug substance within the NP, provided entrapment is efficient, intracellular delivery is expected to deliver a sizeable dose if taken into the cytoplasm. Park *et al*. (2002) demonstrated an increase in therapeutic index of doxorubicin encapsulated in anti-HER2 immunoliposomes, both by reducing side effects and increasing the anti-tumour activity in a HER2 overexpressing tumour xenograft animal model (9). Also, the authors found that anti-HER2 immunoliposomes mediate intracellular drug delivery in HER2-overexpressing tumour cells *in vivo* and suggested that the therapeutic advantage obtained with doxorubicin encapsulated in anti-HER2 immunoliposomes is derived from this targeted internalisation approach. Alternative approaches have examined the direct coupling of drugs to targeting ligands (drug conjugates), which is generally limited by coupling capacity, limited to a few drug molecules per ligand. It follows that the drug-ligand conjugation approach requires high ligand concentrations to achieve effective doses (25,26).

NP with a typical mean diameter of approximately 120 nm, such as those manufactured in this work, are too massive to diffuse passively through the lipid bilayer. The most obvious approach to overcome this challenge is to manufacture the NP in such a way that it both targets and binds to a membrane component that is itself immediately triggered to internalise. If the binding between NP, ligand and receptor is sufficiently robust to maintain the integrity of the complex, then it is again feasible to propose that internalisation will drag the entire construct into the cell. If an alternative approach is taken and a target receptor is chosen that does not internalise, then bound NP will remain immobilised on the external cell surface, where drug release will take place in an extracellular manner, allowing distribution to surrounding, possible healthy, cells (Fig. 1b). Furthermore, targeting non-internalising receptors will create a situation where subsequent concentrations in the cytoplasm will rely on simply the membrane diffusion properties of the drug.

There is no guarantee that non-specific attachment of NP to a cell surface will result in internalisation. The molecular mechanisms mediating the endocytosis of NP are dependent on size. NP as large as 500 nm can be internalised by non-phagocytic cells via an energy dependent process. Smaller NP with a diameter of less than 200 nm are internalised via clathrin-coated pits, while their larger counterparts are internalised via caveolae membrane invaginations (27,28). Slow rates of cellular processing have been demonstrated for clathrin-mediated uptake of NP with a mean diameter of 200 nm (29) and so it is likely that diameters must be kept lower. Indeed, in this work, the NP produced were intentionally kept at approximately 100 nm, as shown in Table I, making them suitable for targeting endocytotic receptors. This control in size was dictated in part by the choice of solvents used in the initial stages of the work (30). However, as seen in Fig. 5b, non-specific attachment of NP within the optimum size range does not lead to substantive nanoparticulate uptake in the MEF cell line. It should be emphasised that size measurements were preformed before antibody attachment. It is reasonable to suggest that following conjugation, the average diameter would increase. As the molecular diameter of a typical IgG has been reported to be as much as 33 nm (31), then peripheral conjugation could make a sizable contribution to the original size of the nanoparticulate core, which may itself be around 120 nm.

The approach taken in this work was to target the siglec-7 receptor, a member of a family of receptors previously shown to internalise upon attachment. This was a similar strategy to that of Nobs *et al*. (32) who, although using a different method of antibody attachment, demonstrated highly selective targeting by biodegradable poly(lactide) nanoparticles *in vitro* to the SKOV-3 (HER2 positive) and Daudi lymphoma (CD20 positive) cell lines. Targeting was mediated by anti-HER2 (trastuzumab) and anti-CD20 (rituximab) monoclonal antibodies, respectively, grafted unto the NP surface using Neutravidin™-biotin approach. In contrast to this previous approach, antibody attachment in this work was mediated by carbodiimide-activated amide formation and it is important this process preserves both the functionality and orientation of a sufficient number of antibodies, correctly orientated with outwardly projecting F_{ab} regions, on the nanoparticulate surface. Viability was ascertained by the ability of the antibody to interact with its cognate antigen using an ELISA. The results presented in Figs. 3 and 4 show that the conjugation procedure was adequately innocuous, allowing the activity of a sufficient number of peripheral siglec-7 antibody to be maintained, permitting efficient and selective binding to its antigen in a dose dependent manner. Estimates place the retention of antibody activity to be approximately 10% (Fig. 3c).

There are three possibilities for the reduction in antibody binding observed in these investigations. First, some of the antibody binding sites at the complementarity determining region (CDR) will be inactivated as a result of conjugation to the nanoparticles (NP). Second, some of the F_c epitope on the siglec antibody will be modified by the conjugation and, thus, masked to recognition by the secondary anti-rabbit antibody-HRP conjugate. Third, the conjugation of a large number of antibodies to the surface of the NP may cause steric hindrance. This hindrance may prevent the siglec antibody from recognising its antigen on the plate or prevent access of the secondary antibody to its epitope on the F_c of the siglec antibody. Therefore, the inactivation of antibody binding may be due to more than one contributing factor. It should be remembered that the results in Fig. 5 show an intense cytoplasmic staining, which indicated that NP were able to get inside the targeted MEF cells efficiently. So, it can be concluded that a drop to 10% of the original binding is still enough to bring about internalisation.

The method chosen for conjugation was based upon the water-soluble carbodiimide/NHS procedure, which requires an existing carboxylic acid grouping density accessible on the nanoparticles surface. This was done by varying the type of PLGA used to prepare the NP core, so that NP formulated using 100% RG 502 H showed higher anti-siglec-7 antibodies attachment compared to NP prepared with less carboxylic acid density (20% RG 502 H). This novel approach imparts a way to alter the available attachment points for conjugation and can be used to alter the antibody density, as shown in Table I. It should also be mentioned that chemical conjugation is likely to produce a more durable and resilient immunologically active surface on the NP when compared to that formed using physical adsorption methods. Furthermore, alterations in the ratio of two PLGA used in this study will have implications for drug release from the loaded core. Although not investigated in this work, it has been described for celecoxib release from PLGA NP made using ratios of RG 502 H and RG 505 S, where a more rapid profile was observed when more of the former polymer was used (30). This means that a more rapid drug release may be indirectly associated with NP possessing a higher surface density of Ab.

Fluorescent cell images of mouse embryonic fibroblasts incubated with NR-loaded NP (Fig. 5) showed that both the siglec receptor and the antibody-conjugated NP were needed to accumulate at the MEF cells. These results also show that leaching of NR from NP bound to the cell surface, as a possible way for NR to enter the cell, was not occurring. This is unlikely anyway, as NR remains firmly entrapped within PLGA NP and does not release into an aqueous continuous phase (data not shown), especially during short incubation periods, as used in this work. Therefore, the results of this figure demonstrate that NP entry is dependent on the presence of both antibody and antigen and that whole NP internalisation is occurring. Further information on the mechanism on internalisation could be gained by low temperature (energy dependent) and competitive binding studies and could be used to progress the work.

Additional evidence that endocytosis was occurring was obtained by changing the dye in the NP. Endocytosis is usually followed by fusion with lysosomes (33). Activated lysosomes are generally characterised by an internal acidic pH of 4.0–5.5 (34). AO is an acidophilic dye and accumulates in intracellular organelles with such acidic pH (35). The fluorescence of AO shifts to longer wavelengths in acidic environments, resulting in a progressive red shift as the pH in the vesicular compartment falls. Thus, red or orange vesicles are more acidic than yellow ones (36). By using AO within the NP, it is possible to identify the formation of activated lysosomal vesicles and its approximate pH (36). When taken together, AO-loaded NP conjugated to anti-siglec-7 antibodies should become conspicuous as an orange-red colour in the cytoplasm if they are present in the endo-lysosomal space. In Fig. 7b, it is seen that red-orange granules accumulate in MEF cells expressing the siglec receptor and incubated with anti-siglec-7 conjugated to AO-loaded NP, demonstrating the presence of the NP in activated lysosomal compartments. It should be mentioned that the presence of green fluorescent protein is problematic in this study, as seen in Fig. 7a and only serves to make interpretation more difficult. The use of AO-loaded NP (Fig. 7d) gave a clearer picture when only the red fluorescence was considered, but suffers an obvious drawback in not indicating its environmental pH.

The findings of this work raise some interesting points. Now that loaded NP are present intracellularly, the next step of the process, namely drug release into the cytoplasm must be considered. Assuming any payload drug can survive the acidic environment of the endosome, it should be gradually released into the cytosol by diffusion from these vesicles. The ability of NP themselves to survive and escape the endo-lysosomal vesicles was found to be dependent on the surface charge of the NP (37). Those which show a transition in their surface charge from an anionic (at pH 7) to a cationic character in the acidic endosomal pH (pH 4–5) were found to escape the endosome. Conversely, NP which remained negatively charged at pH 4 were retained (37). Clearly, by varying the surface charge, it is possible to direct NP to either lysosomes or cytoplasm. The results in Table I show that the immunonanoparticles prepared in this work were cationic at pH 7.4. In having this slight positive charge, acidification will only serve to enhance this property, so leading feasibly to enhanced escape. Work is currently underway to evaluate if the zeta potential changes when placed into an acidic medium.

The endocytosis approach can help in overcoming such difficulties, such as potentially overcoming multidrug resistance effects seen in some cancer cells. Drug molecules can be detected by P–glycoprotein located in the plasma membrane and removed before eliciting any therapeutic effect (38). Given that drug efflux is mediated by P–glycoprotein pumping, an effect located around the plasma membrane, then it is an intriguing proposal that drug entrapped within a NP are effectively hidden from this problematic effect. Internalised NP will be able to release drug within the cytoplasm or endosomal vesicles, thereby increasing its effectiveness (10).

In conclusion, the results from this study show that it is possible to manufacture a nanoparticulate carrier, entrapping a model payload, that presents superficial and variable carboxyl chemistry. This can be used to attach antibodies, in this case anti–siglec–7, with preservation of binding activity. Furthermore, following binding the entire antibody–NP construct is internalised and localising in the activated lysosomal compartments. Further studies are under way to evaluate the effect this aggressive pH has on the stability of entrapped NP and whether a therapeutic payload can escape into the cell cytosol and elicit a cellular response.

REFERENCES

1. J. K. Vasir and V. Labhasetwar. Targeted drug delivery in cancer therapy. *Technology in Cancer Research and Treatment* **4**:363–374 (2005).
2. P. A. McCarron, S. A. Olwill, W. M. Marouf, R. J. Buick, B. Walker, and C. J. Scott. Antibody conjugates and therapeutic strategies. *Mol. Interv.* **5**:368–380 (2005).
3. W. L. Monsky, D. Fukumura, T. Gohongi, M. Ancukiewcz, H. A. Weich, V. P. Torchilin, F. Yuan, and R. K. Jain. Augmentation of transvascular transport of macromolecules and nanoparticles in tumors using vascular endothelial growth factor. *Cancer Res.* **59**:4129–4135 (1999).

4. R. Durand, M. Paul, D. Rivollet, R. Houin, A. Astier, and M. Deniau. Activity of pentamidine-loaded methacrylate nanoparticles against *Leishmania infantum* in a mouse model. *Int. J. Parasitol.* **27**:1361–1367 (1997).
5. D. C. Drummond, K. Hong, J. W. Park, C. C. Benz, and D. B. Kirpotin. Liposome targeting to tumors using vitamin and growth factor receptors. *Vitam. Horm.* **60**:285–332 (2001).
6. P. D. Senter and C. J. Springer. Selective activation of anticancer prodrugs by monoclonal antibody–enzyme conjugates. *Adv. Drug Deliv. Rev.* **53**:247–264 (2001).
7. Y. Mo and L. Y. Lim. Paclitaxel-loaded PLGA nanoparticles: Potentiation of anticancer activity by surface conjugation with wheat germ agglutinin. *J. Control. Release* **108**:244–262 (2005).
8. C. Farokhzad, J. J. Cheng, B. A. Teply, I. Sherifi, S. Jon, P. W. Kantoff, J. P. Richie, and R. Langer. Targeted nanoparticle–aptamer bioconjugates for cancer chemotherapy *in vivo*. *Proc. Natl. Acad. Sci. U. S. A.* **103**:6315–6320 (2006).
9. J. W. Park, K. Hong, D. B. Kirpotin, G. Colbern, R. Shalaby, J. Baselga, Y. Shao, U. B. Nielsen, J. D. Marks, D. Moore, D. Papahadjopoulos, and C. C. Benz. Anti-HER2 immunoliposomes: Enhanced efficacy attributable to targeted delivery. *Clin. Cancer Res.* **8**:1172–1181 (2002).
10. J. Huwyler, A. Cerletti, G. Fricker, A. N. Eberle, and J. Drewe. By-passing of P-glycoprotein using immunoliposomes. *J. Drug Target.* **10**:73–79 (2002).
11. R. H. Jagtvan der, C. C. Badger, F. R. Appelbaum, O. W. Press, D. C. Matthews, J. F. Eary, K. A. Krohn, and I. D. Bernstein. Localization of radiolabeled antimyeloid antibodies in a human acute leukemia xenograft tumor model. *Cancer Res.* **52**:89–94 (1992).
12. L. D. Powell and A. Varki. I-Type lectins. *J. Biol. Chem.* **270**:14243–14246 (1995).
13. S. J. Orr, N. M. Morgan, R. J. Buick, C. R. Boyd, J. Elloitt, J. F. Burrows, C. A. Jefferies, P. R. Crocker, and J. A. Johnston. SOCS3 Target siglec-7 for proteasomal degradation and blocks siglec-7-mediated responses. *J. Biol. Chem.* **282**:3418–3422 (2007).
14. P. R. Crocker. Siglecs: Sialic-acid-binding immunoglobulin-like lectins in cell–cell interactions and signalling. *Curr. Opin. Struck. Biol.* **12**:609–615 (2002).
15. S. J. Orr, N. M. Morgan, J. Elliott, J. F. Burrows, C. J. Scott, D. W. McVicar, and J. A. Johnston. CD33 responses are blocked by SOCS3 through accelerated proteasomal-mediated turnover. *Blood* **10**:1061–1068 (2007).
16. G. Nicoll, T. Avril, K. Lock, K. Furukawa, N. Bovin, and P. R. Crocker. Ganglioside GD3 expression on target cells can modulate NK cell cytotoxicity via siglec-7-dependent and -independent mechanisms. *Eur. J. Immunol.* **33**:1642–1648 (2003).
17. M. Falco, R. Biassoni, C. Bottino, M. Vitale, S. Sivori, R. Augugliaro, L. Moretta, and A. Moretta. Identification and molecular cloning of p75/AIRM1, a novel member of the sialoadhesin family that functions as an inhibitory receptor in human natural killer cells. *J. Exp. Med.* **190**:793–802 (1999).
18. L. Balaian, R. K. Zhong, and E. D. Ball. The inhibitory effect of anti-CD33 monoclonal antibodies on acute myeloid leukaemia (AML) cell growth correlates with Syk and/or ZAP-70 expression. *Exp. Hematol.* **31**:363–371 (2003).
19. E. Nutku, H. Aizawa, S. A. Hudson, and B. S. Bochner. Ligation of siglec-8: A selective mechanism for induction of human eosinophil apoptosis. *Blood* **101**:5014–5020 (2003).
20. C. Vitale, C. Romagnani, A. Puccetti, D. Olive, R. Costello, L. Chiossone, A. Pitto, A. Bacigalupo, L. Moretta, and M. C. Mingari. Surface expression and function of p75/AIRM-1 or CD33 in acute myeloid leukemias: Engagement of CD33 induces apoptosis of leukemic cells. *Proc. Natl. Acad. Sci. U. S. A.* **98**:5764–5769 (2001).
21. E. L. Sievers, F. A. Appelbaum, R. T. Spielberger, S. J. Forman, D. Flowers, F. O. Smith, K. Shannon-Dorcy, M. S. Berger, and I. D. Bernstein. Selective ablation of acute myeloid leukemia using antibody-targeted chemotherapy: A phase I study of an anti-CD33 calicheamicin immunoconjugate. *Blood* **93**:3678–3684 (1999).
22. M. L. Linenberger. CD33-directed therapy with gemtuzumab ozogamicin in acute myeloid leukemia: Progress in understanding cytotoxicity and potential mechanisms of drug resistance. *Leukemia* **19**:176–182 (2005).
23. D. H. Nguyen, E. D. Ball, and A. Varki. Myeloid precursors and acute myeloid leukemia cells express multiple CD33-related Siglecs. *Exp. Hematol.* **34**:728–735 (2006).
24. Y. Mo and L. Lim. Preparation and *in vitro* anticancer activity of wheat germ agglutinin (WGA)-conjugated PLGA nanoparticles loaded with paclitaxel and isopropyl myristate. *J. Control. Release* **107**:30–42 (2005).
25. S. Jaracz, J. Chen, L. V. Kuznetsova, and I. Ojima. Recent advances in tumor-targeting anticancer drug conjugates. *Bioorg. Med. Chem.* **13**:5043–5054 (2005).
26. M. C. Garnett. Targeted drug conjugates: Principles and progress. *Adv. Drug Deliv. Rev.* **53**:171–216 (2001).
27. J. Rejman, V. Oberle, I. S. Zuhorn, and D. Hoekstra. Size-dependent internalization of particles via the pathways of clathrin- and caveolae-mediated endocytosis. *Biochem. J.* **377**:159–169 (2004).
28. M. Koval, K. Preiter, C. Adles, P. D. Stahl, and T. H. Steinberg. Size of IgG-opsonized particles determines macrophage response during internalization. *Exp. Cell Res.* **242**:265–273 (1998).
29. I. S. Zuhorn, R. Kalicharan, and D. Hoekstra. Lipoplex-mediated transfection of mammalian cells occurs through the cholesterol-dependent clathrin-mediated pathway of endocytosis. *J. Biol. Chem.* **277**:18021–18028 (2002).
30. P. A. McCarron, R. F. Donnelly, and W. Marouf. Celecoxib-loaded poly(D,L-lactide-co-glycolide) nanoparticles prepared using a novel and controllable combination of diffusion and emulsification steps as part of the salting-out procedure. *J. Microencapsul.* **23**:480–498 (2006).
31. C. J. Roberts, P. M. Williams, J. Davies, A. C. Dawkes, J. Sefton, J. C. Edwards, A. G. Haymes, C. Bestwick, M. C. Davies, and S. J. B. Tendler. Real-space differentiation of IgG and IgM antibodies deposited on microtiter wells by scanning force microscopy. *Langmuir* **1**:822–826 (1995).
32. L. Nobs, F. Buchegger, R. Gurny, and E. Allemann. Poly(lactic acid) nanoparticles labeled with biologically active Neutravidin™ for active targeting. *Eur. J. Pharm. Biopharm.* **58**:483–490 (2004).
33. J. Panyam, S. Sahoo, S. Prabha, T. Bargar, and V. Labhasetwar. Fluorescence and electron microscopy probes for cellular and tissue uptake of poly(D,L-lactide-coglycolide) nanoparticles. *Int. J. Pharm.* **262**:1–11 (2003).
34. R. G. Anderson and L. Orci. A view of acidic intracellular compartments. *J. Cell Biol.* **106**:539–543 (1988).
35. J. R. Lake, R. W. Van Dyke, and B. F. Scharschmidt. Acidic vesicles in cultured rat hepatocytes. Identification and characterization of their relationship to lysosomes and other storage vesicles. *Gastroenterology* **92**:1251–1261 (1987).
36. C. Butor, G. Griffiths, N. N. Aronson, and A. Varki. Co-localization of hydrolytic enzymes with widely disparate pH optima: Implications for the regulation of lysosomal pH. *J. Cell Sci.* **108**:2213–2219 (1995).
37. J. Panyam, W. Z. Zhou, S. Prabha, S. K. Sahoo, and V. Labhasetwar. Rapid endo-lysosomal escape of poly (D,L-lactide-co-glycolide) nanoparticles: Implications for drug and gene delivery. *FASEB J.* **16**:1217–1226 (2002).
38. A. H. Schinkel and J. W. Jonker. Mammalian drug efflux transporters of the ATP binding cassette (ABC) family: An overview. *Adv. Drug Deliv. Rev.* **55**:3–29 (2003).